energies

MDPI

Article

Evaluation of the Limit State of a Six-Inch Carbon Steel Pipe Elbow in Base-Isolated Nuclear Power Plants

Sung-Wan Kim [1,*], Da-Woon Yun [1], Bub-Gyu Jeon [1], Dae-Gi Hahm [2] and Min-Kyu Kim [2]

[1] Seismic Research and Test Center, Pusan National University, 49 Busandaehak-ro, Yangsan 50612, Korea; ardw818@pusan.ac.kr (D.-W.Y.); bkjeon79@pusan.ac.kr (B.-G.J.)
[2] Smart Structural Safety & Prognosis Division, Korea Atomic Energy Research Institute, 111 Daedeok-daero, 989 beon-gil, Yusung-gu, Daejon 34057, Korea; dhahm@kaeri.re.kr (D.-G.H.); minkyu@kaeri.re.kr (M.-K.K.)
* Correspondence: swkim09@pusan.ac.kr

Abstract: The installation of base isolation systems in nuclear power plants can improve their safety from seismic loads. However, nuclear power plants with base isolation systems experience greater displacement as they handle seismic loads. The increase in relative displacement is caused by the installed base isolation systems, which increase the seismic risk of the interface piping system. It was found that the failure mode of the interface piping system was low-cycle fatigue failure accompanied by ratcheting, and the fittings (elbows and tees) failed due to the concentration of nonlinear behavior. Therefore, in this study, the limit state was defined as leakage, and an in-plane cyclic loading test was conducted in order to quantitatively express the failure criteria for the SCH40 6-inch carbon steel pipe elbow due to low-cycle fatigue failure. The leakage line and low-cycle fatigue curves of the SCH40 6-inch carbon steel pipe elbow were presented based on the test results. In addition, the limit state was quantitatively expressed using the damage index, based on the combination of ductility and energy dissipation. The average values of the damage index for the 6-inch pipe elbow calculated using the force−displacement (P–D) and moment−relative deformation angle (M–R) relationships were found to be 10.91 and 11.27, respectively.

Keywords: nuclear power plant; interface piping system; low-cycle fatigue; carbon steel pipe elbow; limit state

Citation: Kim, S.-W.; Yun, D.-W.; Jeon, B.-G.; Hahm, D.-G.; Kim, M.-K. Evaluation of the Limit State of a Six-Inch Carbon Steel Pipe Elbow in Base-Isolated Nuclear Power Plants. *Energies* **2021**, *14*, 8400. https://doi.org/10.3390/en14248400

Academic Editor: José A. F. O. Correia

Received: 17 September 2021
Accepted: 11 December 2021
Published: 13 December 2021

1. Introduction

Following the Fukushima nuclear power plant accident in Japan, issues concerning the seismic safety of nuclear power plants have been continuously raised [1,2]. In Korea, which is located in regions with low to moderate seismicity, many opinions have been raised that preparation for earthquakes is insufficient, and the country's current seismic design criteria are excessive. It is difficult to object to the opinion that seismic safety must be the top priority in nuclear power plant design, because the ripple effect of seismic damage is difficult to estimate. Therefore, priority must be given to securing seismic performance against the worst case scenario for the seismic design of nuclear power plants in regions with low to moderate and high seismicity [3,4].

In general, base isolation systems are most commonly used to reduce the seismic force of earthquakes on large structures, such as bridges and buildings [5,6]. Base isolation systems increase the natural period of a structure by separating the structure from the ground, thereby reducing the vibration of the structure and improving its seismic performance [7,8]. Thus far, base isolation systems have been recognized as the most reliable seismic response systems because their seismic force reduction effect has been verified. Although base isolation systems significantly contribute to seismic force reduction, the seismic performance of structures with such systems must be re-evaluated as new systems are added to such structures [9,10].

The application of base isolation systems to nuclear power plants has been discussed as an effective method for improving the seismic performance of nuclear power plants [11–13]. Such a method can improve the seismic safety of structures and systems in nuclear power plants that require a seismic design for safe shutdown earthquakes (SSEs) or more intense activity [14–16]. A wide range of studies on the method have been conducted because it can also solve problems, such as the seismic characteristics of the nuclear power plant's installation site [17–19]. Base-isolated nuclear power plants include the Cruas Nuclear Power Plant in France and the Koeberg Nuclear Power Station in South Africa [20,21]. Neoprene pads and reinforced elastomer pads were used for them, respectively. Both power plants are of the pressurized water reactor type, and their SSE is 0.3 g. Several studies have been conducted in order to apply base isolation systems to more nuclear power plants. The U.S. Nuclear Regulatory Commission (NRC) conducted research in order to prepare the technical standards for the application of base isolation systems to nuclear power plants in the country [22]. The Japan Nuclear Energy Safety Organization (JNES) constructed a full-scale model in which base isolation systems were applied to the control room of a nuclear power plant, and a shaking table test was conducted in order to evaluate the seismic stability of the model [23]. In Korea, various experimental and analytical studies have been conducted on the application of base isolation systems to Advanced Power Reactor 1400 (APR1400) in order to reinforce the safety of nuclear power plants in the country [24,25].

The seismic design of the interface piping system, which is supported by structures with and without base isolation systems, is necessary for the design of base-isolated nuclear power plants. Under seismic loads, the interface piping system is deformed due to the large relative displacement between the structures with and without base isolation systems. The interface piping system undergoes an excited state due to the two structures with different vibration characteristics [26]. Due to the occurrence of large relative displacement, the interface piping system may not meet the required seismic performance if it is designed in the same manner as the nuclear power plants without base isolation systems. For the seismic design of the interface piping system, it is necessary to consider the degree of stiffness that can accommodate the inertial force response caused by the different characteristics of the structures with and without base isolation systems, as well as the degree of flexibility that can allow a large relative displacement between the structures caused by seismic loads.

In order to secure the seismic safety of the interface piping system, its seismic performance must be verified, because the occurrence of a large relative displacement is expected [27–29]. In general, the interface piping system consists of straight pipes and fittings (elbows and tees). Previous studies have found that the failure mode of the interface piping system is low-cycle fatigue failure accompanied by ratcheting and that the elements that fail due to the concentration of nonlinear behavior are the fittings [30–33]. In order to evaluate the probabilistic seismic safety of nuclear power plants, research was conducted to define the quantitative failure criteria for the fittings of the interface piping system.

In nuclear power plants, a representative interface piping system, which connects base-isolated structures to non-base-isolated structures, is the main steam line. Test specimens were prepared by referring to the size of the main steam lines in the nuclear power plants of Korea. Since it is difficult to conduct the low-cycle fatigue test for real-scale pipes due to the size of the experimental site and limitations of the equipment, the limit state is assessed by using pipes smaller than the real-scale pipes in most cases. It was found that a scale model was more favorable for simulating the behavior of a prototype as the scaling factor increased and that the behavior of a steel pipe prototype could be simulated well if the scaling factor was 1:6 or higher [34]. In a previous study, the benchmark model of the 12-inch pipe elbow provided by NRC-BNL was considered as a prototype, and research was conducted on a one-quarter scale 3-inch pipe elbow [26]. Since the target of this study was pipes that are 30 inches or larger, the low-cycle fatigue test was conducted by using a 6-inch pipe elbow that could represent the behavior of real-scale pipes.

The test specimen was fabricated by welding an SCH40 6-inch carbon steel pipe elbow with an angle of 90 degrees to the straight pipes. An in-plane cyclic loading test was conducted by using constant amplitudes in various magnitudes until the occurrence of a leakage, which was the limit state of the test specimen. An image measurement system was applied because of the difficulty of measuring the moment and the deformation angle required to define the failure criteria using conventional sensors [33]. The low-cycle fatigue life of the SCH40 6-inch pipe elbow was presented considering various loading amplitudes. The damage index was calculated by using the force−displacement (P–D) and moment−relative deformation angle (M–R) relationships, and the results were compared. The damage indices for the P–D and M–R relationships confirmed that the limit state of the test specimen could be quantitatively expressed. It was also found that the standard deviations of the damage indices could express uncertainties about the capacity of the test specimen and the input load.

2. Methods

2.1. Expeimental Set-Up

In an interface piping system with base isolation systems, the support, brittle connections, and fittings are representative elements vulnerable to seismic loads. There is no brittle connection in the piping system of the safety class of nuclear power plants [35], and the support was not considered because it is usually constrained with a degree of freedom in the finite element model for seismic safety assessment. Therefore, in this study, the pipe elbow, which is a fitting, was selected as an element vulnerable to seismic loads. A 90-degree long pipe elbow, which is a fitting in the interface piping system, and two straight pipes were fabricated as the test specimen. The limit state of the pipe elbow under low-cycle fatigue was evaluated as shown in Figure 1. The test specimen was fabricated by welding straight pipes, whose length was approximately three times their outer diameter, to both ends of the pipe elbow with a radius of curvature of 216.4 mm. The sufficiently long straight pipes were connected in such a way that plastic deformation was concentrated on the pipe elbow. For the test specimen, the straight pipes were ASME 6-inch SCH40 SA 106 Gr. B pipes, and the pipe elbow was an ASME 6-inch SCH40 A234 WPB pipe. The pipe elbow had an outer diameter of 168.3 mm and a thickness of 7.11 mm. Connection jigs with a Φ30 hole and a thickness of 25 mm were welded to both ends of the test specimen to realize a pin connection. Each jig and the pins for connecting them were fabricated with high precision to minimize tolerance and maximize the accuracy of the experiment.

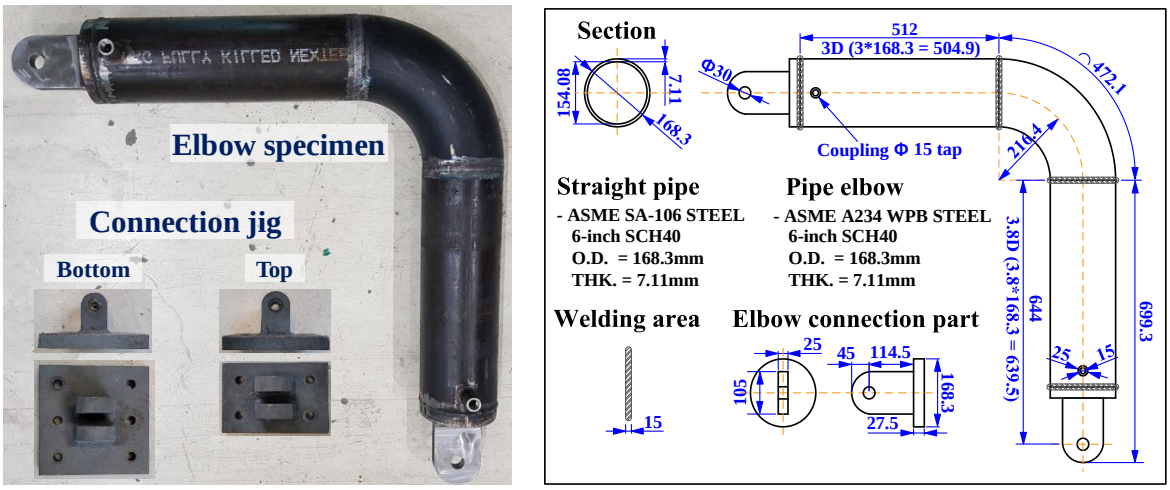

Figure 1. Test specimen composed of a 90-degree pipe elbow and straight pipes.

2.2. Test Procedure and Measurement

A shaking table test or cyclic loading test on the pipe elbow was used in the majority of the experimental studies to evaluate the limit state of the piping under low-cycle fatigue. These tests aim to provide data for updating the finite element model and failure criteria for seismic performance assessment. The tests must be conducted by simulating the service conditions as closely as possible, but the experimental conditions need to be simplified due to the limitations in the experimental facilities and equipment. In general, leakage is examined, and the influence of the internal pressure is considered in the experimental studies in order to evaluate the limit state of the nuclear power plant piping system. The inside of the pipe is filled with room temperature water and the internal pressure is applied and maintained using a hydraulic machine [36–39].

In this study, a cyclic loading test with a constant amplitude was conducted until leakage caused by through-wall cracks occurred in the pipe elbow of the test specimen. In order to examine the leakage caused by the through-wall cracks, the interior of the test specimen was filled with water prior to the test, and an internal pressure of 3 MPa was applied using an air booster. The internal pressure was maintained during the test. In order to minimize the experimental variables, loading was applied in the in-plane direction as shown in Figure 2a to prevent the generation of the moment in the support and torsion of the test specimen and to concentrate the nonlinear behavior on the pipe elbow at the center of the test specimen. The loading amplitude was defined as ±40 mm or higher to allow sufficient plastic behavior at the pipe elbow, and the in-plane cyclic loading test was conducted by adding ±20 mm to consider the elastic–plastic behavior. Therefore, the loading amplitude was increased by ±20 mm from ±20 to ±120 mm. For the in-plane cyclic loading test, the 1000-kN universal testing machine (UTM) of the Seismic Research and Test Center of Korea was used, and its maximum stroke was ±150 mm.

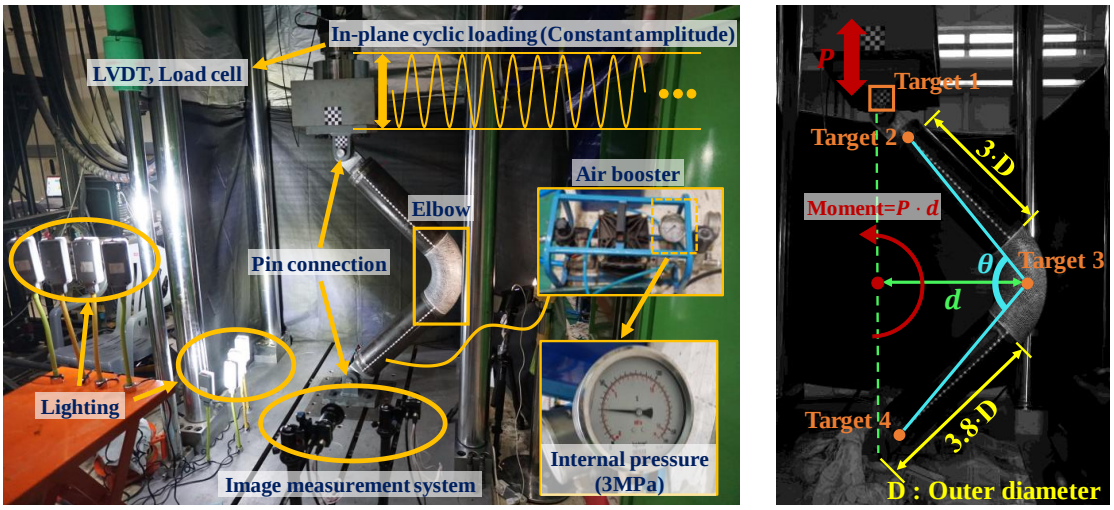

(**a**) (**b**)

Figure 2. Experimental set-up. (**a**) Test specimen installed in UTM. (**b**) Positions for measuring the moment and deformation angle using the image measurement system.

Figure 2b shows the positions of the targets for the measurement of the loading displacement using the UTM, as well as the moment and deformation angle of the test specimen using an image measurement system. The image measurement system used was a complementary metal-oxide-semiconductor (CMOS) camera (IMB-7050G, IMI Tech, Gyeunggi-do, Korea) with a laptop for portability and easy installation. The CMOS camera and laptop performed data transfers by using a universal serial bus (USB) connection. In order to measure the moment, the loading displacement of the UTM and the applied load were required. As shown in Figure 2b, the displacement measured with the image measurement system and from the linear variable differential transformer (LVDT) installed

inside the UTM were compared and synchronized by installing target1 on the jig for the UTM connection [40,41]. In addition, the moment ($M = p \cdot d$) was obtained by multiplying the horizontal distance between target1 and target3 (the center of the elbow), d, by the load measured from the load cell inside the UTM. The deformation angle was calculated by assuming the coordinates of the pixels of target2, target3, and target4 to be straight lines, as shown in Figure 2b. Images of 5472 × 3648 pixels were acquired at 2 frames per second by using the image measurement system, and the UTM applied loading with displacement control at a rate of 40 mm/min. The data acquisition rate was 10 Hz.

3. Test Results

3.1. Low-Cycle Fatigue Life

The seismic loads acting on the interface piping system had the characteristics of relative displacement, and it was found that the elements that failed due to the concentration of nonlinear behavior were the fittings. Under seismic loads, the failure mode of the pipe elbow, which is a fitting in the interface piping system, is low-cycle fatigue failure caused by ratcheting behavior. Therefore, in this study, an in-plane cyclic loading test was conducted in order to define the low-cycle fatigue life of the test specimen under seismic loads from the M–R relationship. In the in-plane cyclic loading test, the failure mode of the pipe elbow was the leakage caused by the through-wall cracks that occurred under low-cycle fatigue. The leakage occurred at a position close to the inner curve of the pipe elbow arch (intrados) in the crown of the pipe elbow, as shown in Figure 3. In addition, Figure 3 shows that the leakage occurred at the pipe elbow of the test specimen due to the through-wall cracks at loading amplitudes of ±20 mm and ±120 mm.

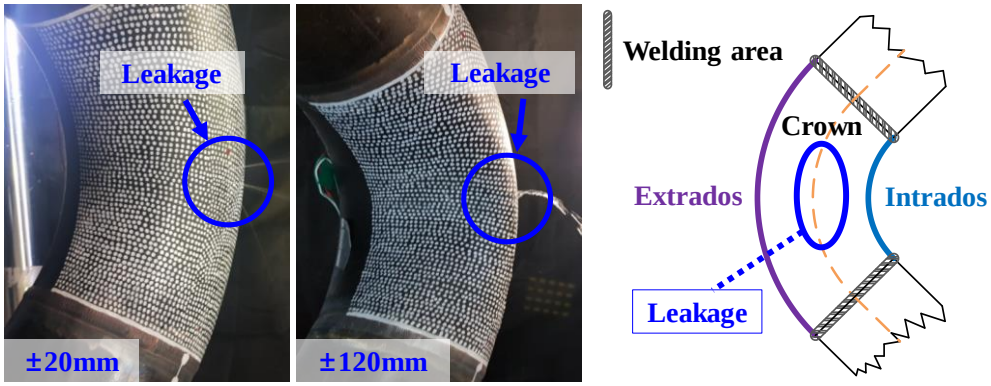

Figure 3. Position of the through-wall cracks (the limit state of the pipe elbow).

The displacement behavior of a structure due to external loads is an indicator of problems with the stability and performance of the structure. However, the use of such an indicator is limited due to many practical difficulties that depend on the measurement conditions. The image measurement system was applied in this study because it was difficult to measure the displacement behavior of the test specimen using conventional sensors. The deformed shape was calculated by using the coordinates of the pixels of the targets in the test specimen. Figure 4 shows the original mode (before the test), the opening mode (tension), and the closing mode (compression) calculated by using the measured coordinates of the pixels. The deformed shape was calculated in the cycle immediately before the occurrence of the leakage by assuming the coordinates of the pixels to be straight lines. The deformed shape was found to be asymmetrical, as shown in Figure 4. Meanwhile, Figure 5 shows the displacement response measured at each target in the test specimen when the loading amplitudes were ±80 mm and ±120 mm.

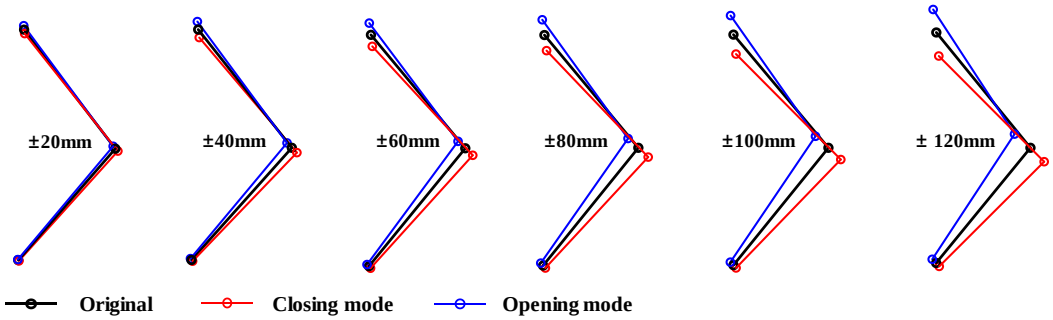

Figure 4. Deformed shape of the test specimen, measured using the image measurement system at each loading amplitude.

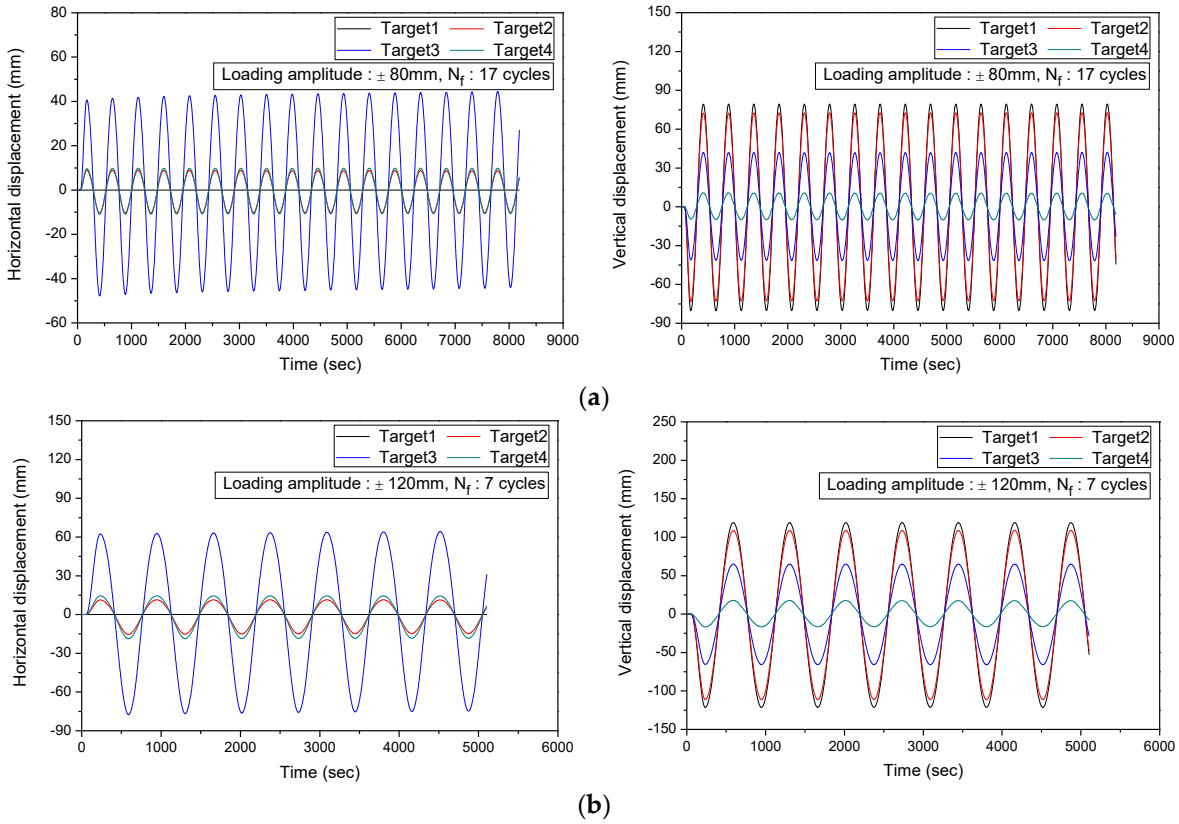

Figure 5. Displacement response measured at each target in the test specimen. (**a**) Displacement response measured in the case with a loading amplitude of ±80 mm. (**b**) Displacement response measured in the case with a loading amplitude of ±120 mm.

In Figure 5, target2 and target4, which are symmetrical points of the test specimen, exhibited no significant differences in horizontal displacement but showed significant differences in vertical displacement. Figures 4 and 5 confirmed that the change in geometry in the vertical direction was larger in the upper part of the test specimen than in the lower part.

Table 1 shows the number of cycles to failure, the average energy for one cycle, the moment range, and the relative deformation angle range when the leakage occurred in the pipe elbow of 12 test specimens at each loading amplitude in the in-plane cyclic loading test. As shown in the table, the number of cycles to failure (N_f) ranged from 7.00 to 347.50 cycles. The average energy for one cycle ranged from 0.70 to 45.01 kN·m for P–D and from 0.72 to 25.64 kN·m for M–R. The moment ranged from 66.60 to 135.11 kN·m, and the relative deformation angle ranged from 0.066 to 0.419 rad. The average energy for one cycle calculated from the P–D relationship and that calculated from the M–R relationship

were found to have been similar, as their difference was less than 3%. Since the energy for one cycle could determine the degree of plastic deformation, the low-cycle fatigue life decreased as the energy for one cycle increased.

Table 1. Number of cycles to failure, average energy for one cycle, moment range, and relative deformation angle range.

Loading Amplitude (mm)	N_f	Average Energy for One Cycle (kN·m)			Range	
		P–D	M–R	Difference (%)	Moment (kN·m)	Relative Deformation Angle (Rad)
±20	347.50	0.70	0.72	2.02	72.36	0.066
	318.00	0.88	0.86	1.86	66.60	0.067
±40	101.25	4.31	4.42	2.60	82.58	0.14
	91.50	4.17	4.13	0.94	86.13	0.138
±60	42.25	8.77	8.77	0.04	98.29	0.204
	41.25	9.12	9.03	1.01	100.83	0.205
±80	20.00	15.12	15.20	0.55	110.54	0.279
	17.00	13.86	13.57	2.09	104.76	0.28
±100	12.00	19.81	20.22	2.09	121.09	0.35
	15.00	21.00	21.61	2.87	129.48	0.346
±120	9.25	25.89	25.64	0.96	134.68	0.419
	7.00	26.34	25.29	0.18	135.11	0.415

Figure 6 shows the hysteresis loops for the P–D and M–R relationships of a representative test specimen at each loading amplitude measured in the in-plane cyclic loading test. The area of the hysteresis loop is the energy dissipated by plastic deformation. It was confirmed that energy dissipation increased as the loading amplitude increased. In addition, Figure 6 confirms that the hysteresis loops for the P–D and M–R relationships were asymmetrical, because the deformed shape of the test specimen had different behaviors in the closing and opening modes.

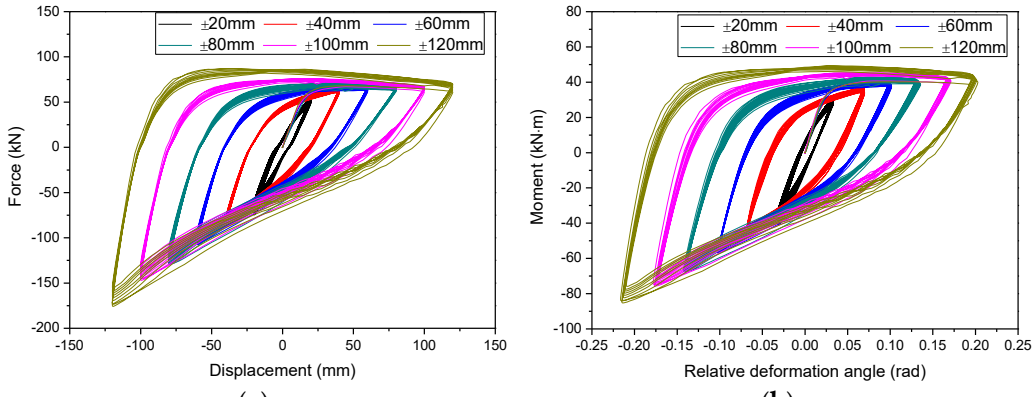

(**a**) (**b**)

Figure 6. Hysteresis loops for the P–D and M–R relationships. (**a**) Hysteresis loop for the P–D relationship. (**b**) Hysteresis loop for the M–R relationship.

The leakage line is the linear representation of the time at which leakage occurred in the pipe elbow in the experiment results. In addition, the leakage line is used as important data for the design and safety assessment of the pipe by identifying its fatigue life, considering the size of the cyclic loading. Figure 7 shows the leakage line obtained using the relationship between the moment range (M_R) and the relative deformation angle range (θ_R) in the low-cycle fatigue test. Equation (1) computes the average regression curve by using the least squares method. In the equation, the coefficient of determination (R^2) is

0.98 or higher, which indicates a linear relationship between the moment range and the relative deformation angle range.

$$M_R = 186.27 \cdot \theta_R + 58.38, R^2 = 0.98 \quad (1)$$

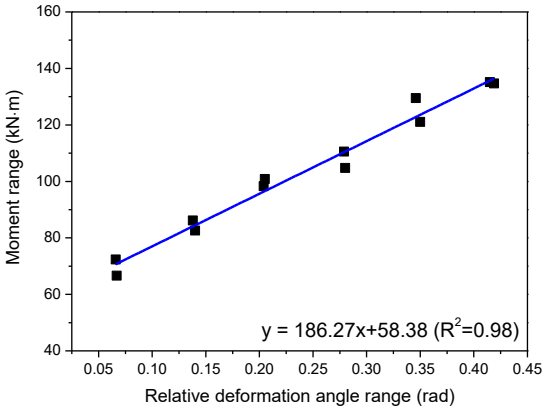

Figure 7. Leakage line for the relationship between the moment range and the relative deformation angle range.

In order to examine the low-cycle fatigue life of the test specimen, the low-cycle fatigue curves for the moment range and the relative deformation angle range are shown in Figure 8, according to the number of cycles to failure. Equations (2) and (3) compute the relationships for the low-cycle fatigue life of the test specimen shown in Figure 7. The low-cycle fatigue lives for the moment range and the relative deformation angle range were found to be predictable by using Equations (2) and (3). The data following the leakage, which was the failure mode of the test specimen, are represented by the low-cycle fatigue curves in Figure 8. They exhibited very high reliability, as their coefficient of determination was 0.94 or higher.

$$M_R = 192.97 N_f^{-0.18}, R^2 = 0.94 \quad (2)$$

$$\theta_R = 1.06 N_f^{-0.44}, R^2 = 0.98 \quad (3)$$

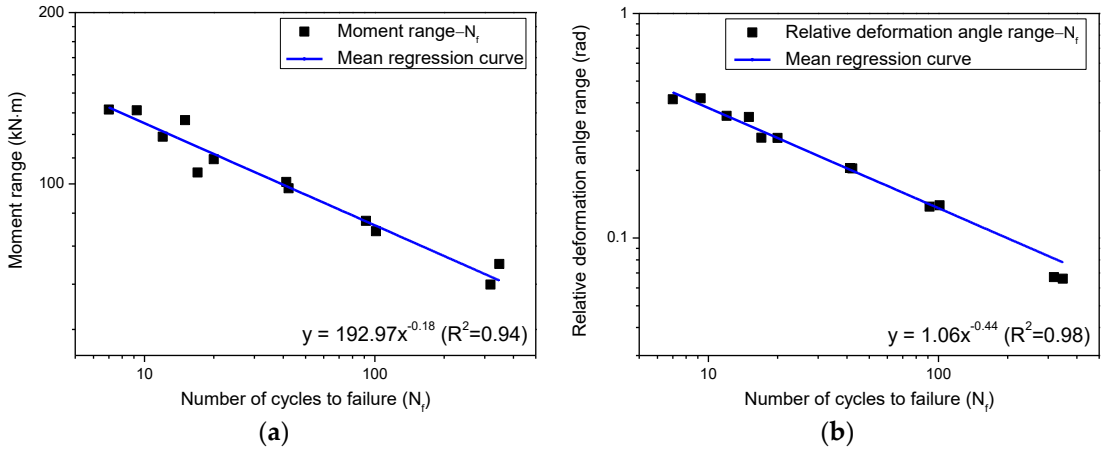

Figure 8. Low-cycle fatigue life. (**a**) Low-cycle fatigue curve for the relationship between the moment range and the number of cycles to failure. (**b**) Low-cycle fatigue curve for the relationship between the relative deformation angle range and the number of cycles to failure.

3.2. Failure Criteria Evaluation

An element of an interface piping system that is vulnerable to seismic loads, a method of simply and directly calculating the damage index for the limit state of the pipe elbow, is required in order to analyze the probabilistic seismic fragility of the pipe elbow [26,42]. For the damage index calculated using the P–D relationship, the direction of the load that acted on the pipe elbow in the experiment may not have coincided with the direction of the load that acted on the pipe elbow in the finite element model of the interface piping system. Analysis of the damage index calculated using the M–R relationship was simpler than the analysis of the damage index calculated using the P–D relationship. Based on the analysis results, the damage index of the pipe elbow could be directly calculated.

Failure was found to occur due to low-cycle fatigue accompanied by ratcheting in the interface piping system, with the pipe elbow as the element that was vulnerable to seismic loads. In this study, an attempt was made to quantitatively express the failure criteria for the test specimen using damage indices. In order to examine the possibility of quantitatively expressing the failure criteria for the test specimen using the M–R relationship, the damage index calculated using the M–R relationship was compared with that calculated using the P–D relationship. Equations (4) and (5) compute the damage indices of Banon by nonlinearly combining the ductility index and the energy dissipation index [43,44]. Equation (4) computes the damage index for the P–D relationship, and Equation (5) computes the damage index for the M–R relationship. The constants c and d in Equations (4) and (5) were set as 3.3 and 0.21, respectively, based on the results of previous studies [26,42].

In Equations (4) and (5), D_y is the yield displacement, F_y is the yield force, D_i is the displacement amplitude of the i-th cycle, $E_{i(P-D)}$ is the energy dissipation for the P–D relationship, M_y is the yield moment, θ_y is the yield relative deformation angle, θ_i is the relative deformation angle amplitude of the i-th cycle, and $E_{i(M-R)}$ is the energy dissipation for the M–R relationship:

$$D_{P-D} = \sqrt{\left(\max\left(\frac{D_i}{D_y} - 1\right)\right)^2 + \left(\sum_{i=1}^{N} c\left(\frac{E_{i(P-D)}}{F_y D_y}\right)^d\right)^2} \quad (4)$$

$$D_{M-R} = \sqrt{\left(\max\left(\frac{\theta_i}{\theta_y} - 1\right)\right)^2 + \left(\sum_{i=1}^{N} c\left(\frac{E_{i(M-R)}}{M_y \theta_y}\right)^d\right)^2} \quad (5)$$

In order to calculate Banon's damage indices using Equations (4) and (5), the yield point (D_y, F_y, M_y, θ_y), which is the limit load, must be defined. In a previous study, the representative yield point of each test specimen was defined by using the tangent intersection (TI) method in the mean regression curves of their first cycles [42]. For the TI method, different yield points can be calculated depending on the method of defining the tangent of the slope in the plastic region [45]. This indicates that the position of the yield point may vary, depending on the subjective judgment of the engineer for the TI method. Therefore, in this study, the yield point was defined by using the twice elastic slope (TES) method as shown in Figure 9. In the ASME Boiler & Pressure Vessel Code, the collapse load point is defined by using the TES method as the limit state of the piping and pressure vessels [46]. A regression line was drawn in the elastic region of the P–D curve by using the least squares method, and the resulting angle was referred to as θ. In addition, a line was drawn with an angle Φ that became $2\tan\theta$ using Equation (6). The point at which this line met the P–D curve was the collapse load point:

$$\Phi = \tan^{-1}(2\tan\theta) \quad (6)$$

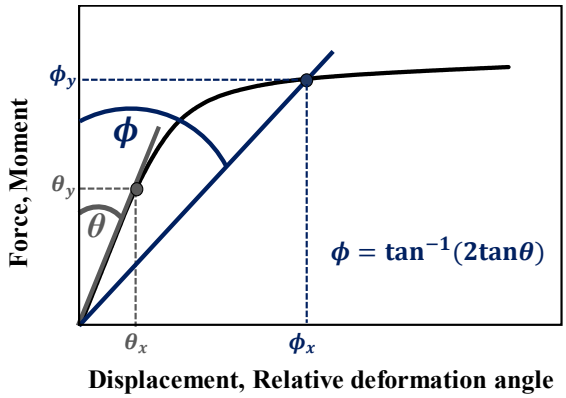

Figure 9. TES method.

In a previous study, the yield point had one representative value, and it was applied to all the test specimens in the same manner [42,45]. Banon's damage index, however, is based on the nonlinear combination of the ductility index and the energy dissipation index. As a result, when one representative value is defined and used for the yield point, the energy dissipation index becomes a variable for calculating the damage index. Therefore, the yield point and the dissipated energy were calculated for each test specimen in order to consider the influence of the material variability, fabrication error, and input load. Figure 10 shows the results of the application of the TES method to the loading amplitudes of ±20 mm and ±40 mm. The TES method was found to be applicable when the loading amplitude was ±40 mm, as shown in Figure 10b, but not when the loading amplitude was ±20 mm, as shown in Figure 10a. Therefore, when the loading amplitude was ±20 mm, the maximum value was used as the yield point, as shown in Figure 10a. When the loading amplitude was ±20 mm, cumulative plastic deformation occurred when the yield load was exceeded, but the behavior in the elastic–plastic region below the collapse load point was observed. In addition, the collapse load point, which is the limit load for seismic design, was found to have been exceeded when the loading amplitude was ±40 mm.

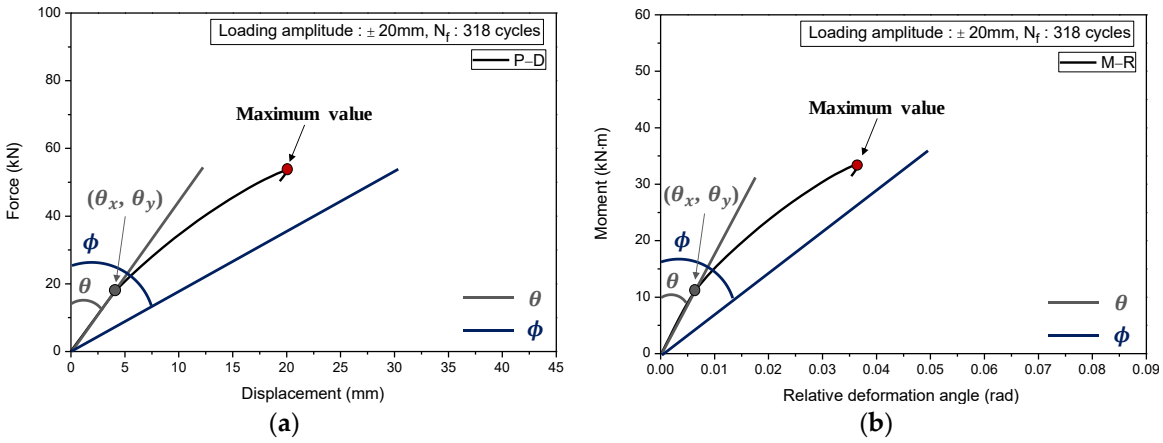

Figure 10. Yield point calculation using the TES method. (**a**) TES method application for the P–D and M–R relationships at a loading amplitude of ±20 mm. (**b**) TES method application for the P–D and M–R relationships at a loading amplitude of ±40 mm.

Figure 11 shows the damage indices calculated by using the P–D and M–R relationships at each loading amplitude. Here, the distribution of the damage index represented the uncertainty about the capacity of each test specimen and the uncertainty about leakage, which was the actual failure at each loading amplitude. The damage indices for each loading amplitude were located within ±2σ (the standard deviation) of the average line. Table 2 further shows the damage indices calculated using the P–D and M–R relationships for each loading amplitude. It shows a difference of 1.33–9.84% between the damage index

calculated using the P–D relationship and that calculated using the M–R relationship and a difference of approximately 5% between the average value of the damage index calculated using the P–D relationship and that of the damage index calculated using the M–R relationship. In Table 3, the standard deviations for the damage indices calculated using the P–D and M–R relationships are shown as 0.82 and 0.66, respectively. It will be possible to use the standard deviation of the damage index in order to consider damage uncertainty when seismic fragility analysis is conducted. These confirm that the damage indices calculated using the P–D and M–R relationships for each loading amplitude converged at a certain level. The standard deviations of the damage indices calculated for each loading amplitude were less than 0.9, which indicates that the average values of the damage indices could be used as representative values to express the leakage caused by the through-wall cracks. In this study, the average value of the damage index was presented as a representative value to express leakage. Engineers, however, will be able to select and use such representative values as the median value, maximum value, and minimum value, other than the average value of the damage index, depending on the purpose. Tables 2 and 3 show that the average damage indices calculated using the M–R relationship were located within ±2σ of the average damage indices calculated using the P–D relationship. This indicates that there were high correlations between the damage indices calculated using the P–D and M–R relationships. It was confirmed that the damage indices calculated using the P–D and M–R relationships quantitatively expressed the leakage of the test specimen caused by through-wall cracks.

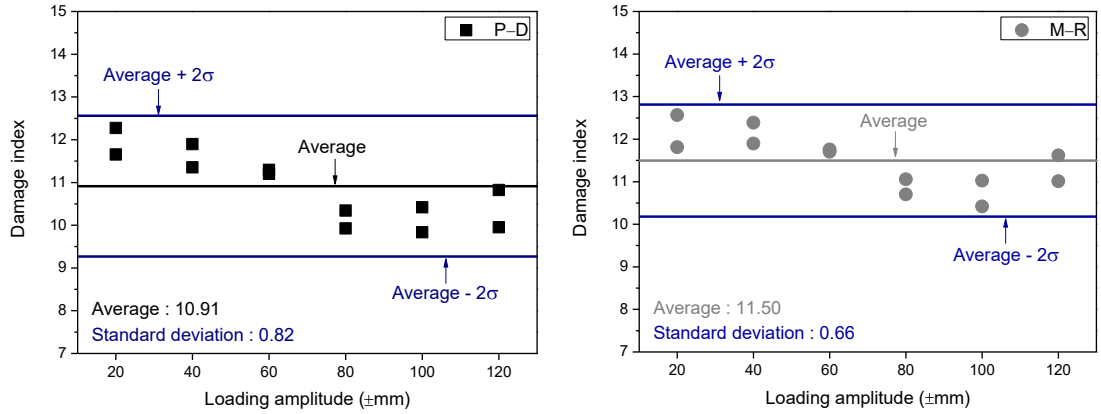

Figure 11. Damage indices for the P–D and M–R relationships. (**a**) Damage index for the P–D relationship. (**b**) Damage index for the M–R relationship.

Table 2. Damage indices calculated by using the P–D and M–R relationships.

Loading Amplitude	Damage Index		
	P–D	M–R	Difference (%)
±20	11.66	11.81	1.33
	12.28	12.57	2.31
±40	11.90	12.38	3.93
	11.35	11.89	4.55
±60	11.20	11.76	4.75
	11.30	11.70	3.47
±80	9.92	10.70	7.26
	10.34	11.06	6.47
±100	9.83	10.42	5.60
	10.42	11.02	5.50
±120	10.82	11.62	6.84
	9.95	11.01	9.84
Average	10.91	11.50	5.06

Table 3. Statistical information on the calculated damage indices.

Statistical Data	Damage Index	
	P–D	**M–R**
average	10.91	11.27
median	11.03	11.39
maximum	12.28	12.44
minimum	9.83	10.17
variance	0.62	0.47
standard deviation	0.82	0.66
average + 2·σ	12.49	12.65
average − 2·σ	9.33	9.89

4. Conclusions

In this study, the low-cycle fatigue life of the SCH40 6-inch carbon steel pipe elbow in the interface piping system of nuclear power plants under seismic loads was presented using the moment–relative deformation angle (M–R) relationship. In addition, the failure criteria for leakage, which was the limit state, were quantitatively expressed using the damage indices that could consider the ductility and energy dissipation for the force–displacement (P–D) and M–R relationships.

The in-plane cyclic loading test was conducted by applying an internal pressure of 3 MPa to the SCH40 6-inch carbon steel pipe elbow in order to present the low-cycle fatigue life of the pipe elbow for the M–R relationship. The loading amplitude was increased by ±20 mm from ±20 to ±120 mm so as to consider the relative displacement generated in the interface piping system under seismic loads. The test was conducted until leakage, which was the limit state of the pipe elbow, occurred as a result of through-wall cracks. Leakage occurred at a position close to the inner curve of the pipe elbow arch in the crown of the pipe elbow, and through-wall cracks propagated from the inside to the outside and in the axial direction. Based on the test results, the highly reliable leakage line and low-cycle fatigue curves were presented by using the relationships between the moment range, relative deformation angle range, and number of cycles to failure.

The failure criteria for the SCH40 6-inch carbon steel pipe elbow were quantitatively expressed by using the damage indices that could consider the combination of ductility and energy dissipation. The average values of the damage indices calculated using the P–D and M–R relationships were found to be 10.91 and 11.27, respectively, thereby showing a difference of approximately 5%. Therefore, when the seismic response of the piping system is analyzed using the finite element model, it will be possible to reduce the analysis procedure by applying the damage index that uses the M–R relationship rather than the damage index that uses the P–D relationship, which makes it difficult to specify the load acting on the pipe elbow. In addition, all the damage indices for each loading amplitude were confirmed to have been located within ±2σ (the standard deviation) of the average line. Moreover, the standard deviations for the damage indices calculated using the P–D and M–R relationships were found to be less than 0.9. This confirmed that the damage indices calculated using the P–D and M–R relationships can quantitatively express the failure criteria for the limit state of the 6-inch carbon steel pipe elbow. In particular, the standard deviation of the damage index can be used as a coefficient that expresses the uncertainty about damage when the seismic vulnerability of steel piping is analyzed.

The leakage line and low-cycle fatigue curves of the SCH40 6-inch carbon steel pipe elbow presented in this study are expected to be used as basic data for predicting the low-cycle fatigue life of the interface piping systems in nuclear power plants. The damage indices calculated using the P–D and M–R relationships may be used as quantitative failure criteria that can express leakage, which is the limit state of the pipe elbow required for reliable seismic fragility analysis. In addition, it will be possible to quantitatively define variability in the damage index, considering the size effect of the 6-inch carbon steel pipe elbow through a comparison with the results of the previous studies conducted on the

3-inch carbon steel pipe elbow. This will make it possible to estimate damage to real-scale pipe elbows from the results of small-sized pipe elbows.

Author Contributions: Conceptualization, S.-W.K. and D.-W.Y.; experimental tests, S.-W.K., D.-W.Y. and B.-G.J.; methodology, S.-W.K., D.-W.Y., B.-G.J., D.-G.H. and M.-K.K.; software, S.-W.K.; validation, S.-W.K. and D.-W.Y.; visualization, S.-W.K. and D.-W.Y.; investigation, S.-W.K., D.-W.Y., B.-G.J., D.-G.H. and M.-K.K.; writing—original draft, S.-W.K. and D.-W.Y.; writing—review and editing, S.-W.K., D.-W.Y. and B.-G.J. All authors have read and agreed to the published version of the manuscript.

Funding: This work was supported by the Korea Institute of Energy Technology Evaluation and Planning (KETEP) and the Ministry of Trade, Industry and Energy (MOTIE) of the Republic of Korea (No. 20201510100010). Moreover, the authors would like to thank the KOCED Seismic Research and Test Center for their assistance with the test equipment.

Institutional Review Board Statement: Not applicable.

Informed Consent Statement: Not applicable.

Data Availability Statement: Not applicable.

Conflicts of Interest: The authors declare no conflict of interest.

Abbreviations

APR1400	Advanced Power Reactor 1400
CMOS	Complementary metal-oxide-semiconductor
JNES	Japan Nuclear Energy Safety Organization
LVDT	Linear variable differential transformer
NRC	Nuclear Regulatory Commission
SSE	Safe shutdown earthquake
TES	Twice elastic slope
TI	Tangent intersection
USB	Universal serial bus
UTM	Universal testing machine
D_i	Displacement amplitude of i-th cycle
D_{M-R}	Damage index for M–R relationship
D_{P-D}	Damage index for P–D relationship
D_y	Yield displacement
$E_{i(M-R)}$	Dissipated energy of i-th cycle by M–R relationship
$E_{i(P-D)}$	Dissipated energy of i-th cycle by P–D relationship
F_y	Yield force
M–R	Moment–relative deformation angle
M_R	Moment range
M_y	Yield moment
N_f	Number of cycles to failure
P–D	Force−displacement
R^2	Coefficient of determination
θ	Angle
θ_i	Relative deformation angle amplitude of i-th cycle
θ_R	Relative deformation angle range
θ_y	Yield relative deformation angle
σ	Standard deviation
Φ	$\tan^{-1}(2\tan\theta)$

References

1. Wang, Q.; Xi, C.; Xu, Y.C. Accident like the Fukushima unlikely in a country with effective nuclear regulation: Literature review and proposed guidelines. *Renew. Sustain. Energy Rev.* **2013**, *17*, 126–146. [CrossRef]
2. Saji, G. Safety goals for seismic and tsunami risks: Lessons learned from the Fukushima Daiichi disaster. *Nucl. Eng. Des.* **2014**, *280*, 449–463. [CrossRef]

3. Stevenson, J.D. Summary of the historical development of seismic design of nuclear power plants in Japan and the U.S. *Nucl. Eng. Des.* **2014**, *269*, 160–164. [CrossRef]
4. Nguyen, D.D.; Thusa, B.; Han, T.S.; Lee, T.H. Identifying significant earthquake intensity measures for evaluating seismic damage and fragility of nuclear power plant structures. *Nucl. Eng. Technol.* **2020**, *52*, 192–205. [CrossRef]
5. Jangid, R.S. Seismic response of isolated bridges. *J. Bridge Eng.* **2004**, *9*, 156–166. [CrossRef]
6. Warn, G.P.; Ryan, K.L. A review of seismic isolation for buildings: Historical development and research needs. *Buildings* **2012**, *2*, 300–325. [CrossRef]
7. Buckle, I.G.; Mayes, R.L. Seismic isolation: History, application, and performance—a world view. *Earthq. Spectra* **1990**, *6*, 161–201. [CrossRef]
8. Makris, N. Seismic isolation: Early history. *Earthq. Eng. Struct. Dyn.* **2019**, *48*, 269–283. [CrossRef]
9. Wongprasert, N.; Symans, M.D. Numerical evaluation of adaptive base-isolated structures subjected to earthquake ground motions. *J. Eng. Mech.* **2005**, *131*, 109–119. [CrossRef]
10. Zhang, J.; Huo, Y. Evaluating effectiveness and optimum design of isolation devices for highway bridges using the fragility function method. *Eng. Struct.* **2009**, *31*, 1648–1660. [CrossRef]
11. Whittaker, A.S.; Sollogoub, P.; Kim, M.K. Seismic isolation of nuclear power plants: Past, present and future. *Nucl. Eng. Des.* **2018**, *338*, 290–299. [CrossRef]
12. Zhou, Z.; Hu, X.; Wong, J. Special issues in the application of seismic isolation to nuclear power plants. *Energies* **2018**, *11*, 2333. [CrossRef]
13. Lo Frano, R. Benefits of seismic isolation for nuclear structures subjected to severe earthquake. *Sci. Technol. Nucl. Install.* **2018**, *2018*, 8017394. [CrossRef]
14. Lo Frano, R.; Forasassi, G. Isolation systems influence in the seismic loading propagation analysis applied to an innovative near term reactor. *Nucl. Eng. Des.* **2010**, *240*, 3539–3549. [CrossRef]
15. Chen, J.; Zhao, C.; Xu, Q.; Yuan, C. Seismic analysis and evaluation of the base isolation system in AP1000 NI under SSE loading. *Nucl. Eng. Des.* **2014**, *278*, 117–133. [CrossRef]
16. Medel-Vera, C.; Ji, T. Seismic protection technology for nuclear power plants: A systematic review. *J. Nucl. Sci. Technol.* **2015**, *52*, 607–632. [CrossRef]
17. Takeda, M.; Ohkawa, Y.; Akutsu, Y. An evaluation method for seismic isolation effect in siting of a nuclear facility. *Reliab. Eng. Syst. Saf.* **1998**, *62*, 241–249. [CrossRef]
18. Kubo, T.; Yamamoto, T.; Sato, T.; Jimbo, M.; Imaoka, T.; Umeki, Y. A seismic design of nuclear reactor building structures applying seismic isolation system in a high seismicity region—a feasibility case study in Japan. *Nucl. Eng. Technol.* **2014**, *46*, 581–594. [CrossRef]
19. Yu, C.C.; Bolisetti, C.; Coleman, J.L.; Kosbab, B.; Whittaker, A.S. Using seismic isolation to reduce risk and capital cost of safety-related nuclear structures. *Nucl. Eng. Des.* **2018**, *326*, 268–284. [CrossRef]
20. Coladant, C. Seismic isolation of nuclear power plants—EDF's philosophy. *Nucl. Eng. Des.* **1991**, *127*, 243–251. [CrossRef]
21. Wang, H.; Weng, D.; Lu, X.; Lu, L. Life-cycle cost assessment of seismically base-isolated structures in nuclear power plants. *Nucl. Eng. Des.* **2013**, *262*, 429–434. [CrossRef]
22. Kammerer, A.M.; Whittaker, A.S.; Constantinou, M.C. *Technical Considerations for Seismic Isolation of Nuclear Facilities (NUREG/CR-7253)*; U.S. Nuclear Regulatory Commission: Rockville, MD, USA, 2019.
23. Japan Electric Association(JEA). *Technical Design Guide for Seismic Isolation of Nuclear Power Facilities*; JEAG4614-2000; Japan Electric Association(JEA): Tokyo, Japan, 2000.
24. Choi, Y.; Park, J.B.; Lee, S.J.; Park, N.C.; Park, Y.P.; Kim, J.S.; Roh, W.J. Seismic analysis of the APR 1400 reactor vessel internals using the model reduction method. *J. Nucl. Sci. Technol.* **2016**, *53*, 1701–1714. [CrossRef]
25. Nguyen, D.D.; Thusa, B.; Park, H.; Azad, M.S.; Lee, T.H. Efficiency of various structural modeling schemes on evaluating seismic performance and fragility of APR1400 containment building. *Nucl. Eng. Technol.* **2021**, *53*, 2696–2707. [CrossRef]
26. Kim, S.W.; Jeon, B.G.; Hahm, D.G.; Kim, M.K. Seismic fragility evaluation of the base-isolated nuclear power plant piping system using the failure criterion based on stress-strain. *Nucl. Eng. Technol.* **2019**, *51*, 561–572. [CrossRef]
27. Hahm, D.G.; Park, J.H.; Choi, I.K. Seismic performance evaluation of piping system crossing the isolation interface in seismically isolated NPP. *J. Earthq. Soc. Korea* **2014**, *18*, 141–150. [CrossRef]
28. Surh, H.B.; Ryu, T.Y.; Park, J.S.; Ahn, E.W.; Choi, C.S.; Koo, J.C.; Choi, J.B.; Kim, M.K. Seismic response analysis of a piping system subjected to multiple support excitations in a base isolated NPP building. *Nucl. Eng. Des.* **2015**, *292*, 283–295. [CrossRef]
29. Kwag, S.Y.; Eem, S.H.; Kwak, J.S.; Lee, H.H.; Oh, J.H.; Koo, G.H. Mitigation of seismic responses of actual nuclear piping by a newly developed tuned mass damper device. *Nucl. Eng. Technol.* **2021**, *53*, 2728–2745. [CrossRef]
30. Vishnuvardhan, S.; Raghava, G.; Gandhi, P.; Saravanan, M.; Goyal, S.; Arora, P.; Gupta, S.K.; Bhasin, V. Ratcheting failure of pressurized straight pipes and elbows under reversed bending. *Int. J. Press. Vessel. Pip.* **2013**, *105–106*, 79–89. [CrossRef]
31. Hassan, T.; Rahman, M.; Bari, S. Low-cycle fatigue and ratcheting responses of elbow piping components. *J. Press. Vessel. Technol.* **2015**, *137*, 031010. [CrossRef]
32. Ravi Kiran, A.; Reddy, G.R.; Agrawal, M.K. Risk-based seismic performance assessment of pressurized piping systems considering ratcheting. *J. Press. Vessel. Technol.* **2020**, *142*, 021902. [CrossRef]

33. Kim, S.W.; Jeon, B.G.; Hahm, D.G.; Kim, M.K. Ratcheting fatigue failure of a carbon steel pipe tee in a nuclear power plant using the deformation angle. *Eng. Fail. Anal.* **2020**, *114*, 104595. [CrossRef]
34. Choi, H.S.; Jeon, B.G.; Firoozabad, E.S.; Kim, N.S. Small scaled model tests for piping components of seismically isolated nuclear power plant. In Proceedings of the SMiRT-23, Manchester, UK, 10–14 August 2015.
35. Electric Power Research Institute. *Seismic Fragility and Seismic Margin Guidance for Seismic Probabilistic Risk Assessments*; EPRI TR-3002012994; Electric Power Research Institute: Palo Alto, CA, USA, 2018.
36. Nakamura, I.; Otani, A.; Shiratori, M. Comparison of failure modes of piping systems with wall thinning subjected to in-plane, out-of-plane, and mixed mode bending under seismic load: An experimental approach. *J. Press. Vessel. Technol.* **2010**, *132*, 0310011–0310018. [CrossRef]
37. Varelis, G.E.; Karamanos, S.A.; Gresnigt, A.M. Pipe elbows under strong cyclic loading. *J. Press. Vessel. Technol.* **2013**, *135*, 11207. [CrossRef]
38. Urabe, Y.; Takahashi, K.; Sato, K.; Ando, K. Low cycle fatigue behavior and seismic assessment for pipe bend having local wall thinning-influence of internal pressure. *J. Press. Vessel. Technol.* **2013**, *135*, 041802. [CrossRef]
39. Nuclear Energy Agency/Committee on the Safety of Nuclear Installations. Integrity of Structures, Final Report of the Project on Metallic Component Margins under High Seismic Loads (MECOS). In *Systems and Components under Design and Beyond Design Loads in Nuclear Power Plants*; Nuclear Energy Agency: Paris, France, 2018.
40. Kim, S.W.; Choi, H.S.; Jeon, B.G.; Hahm, D.G.; Kim, M.K. Strain and deformation angle for a steel pipe elbow using image measurement system under in-plane cyclic loading. *Nucl. Eng. Technol.* **2018**, *50*, 190–202. [CrossRef]
41. Kim, S.W.; Choi, H.S.; Jeon, B.G.; Hahm, D.G. Low-cycle fatigue behaviors of the elbow in a nuclear power plant piping system using the moment and deformation angle. *Eng. Fail. Anal.* **2019**, *96*, 348–361. [CrossRef]
42. Kim, S.W.; Chang, S.J.; Park, D.U.; Jeon, B.G. Failure criteria of a carbon steel pipe elbow for low-cycle fatigue using the damage index. *Thin-Walled Struct.* **2020**, *153*, 106800. [CrossRef]
43. Banon, H.; Biggs, J.M.; Irvine, H.M. Seismic damage in reinforced concrete frames. *J. Struct. Div.* **1981**, *107*, 1713–1729. [CrossRef]
44. Banon, H.; Veneziano, D. Seismic safety of reinforced concrete members and structures. *Earthq. Eng. Struct. Dyn.* **1982**, *10*, 179–193. [CrossRef]
45. Kim, S.W.; Yun, D.W.; Chang, S.J.; Park, D.U. Quantitative limit state assessment of a 3-inch carbon steel pipe tee in a nuclear power plant using a damage index. *Energies* **2020**, *13*, 6395. [CrossRef]
46. American Society of Mechanical Engineers. Section III, Rules for Construction of Nuclear Facility Components. In *ASME Boiler and Pressure Vessel Code*; The American Society of Mechanical Engineers (ASME): New York, NY, USA, 2004.